Materials & Design 230 (2023) 111970

Contents lists available at ScienceDirect

Materials & Design

journal homepage: www.elsevier.com/locate/matdes

Wearable Graphene-based smart face mask for Real-Time human respiration monitoring

Hossein Cheraghi Bidsorkhi *, Negin Faramarzi, Babar Ali, Lavanya Rani Ballam, Alessandro Giuseppe D'Aloia, Alessio Tamburrano, Maria Sabrina Sarto

Department of Astronautical, Electrical, and Energy Engineering (DIAEE), Sapienza University of Rome, via Eudossiana 18, 00184 Rome, Italy
Research Center for Nanotechnology Applied to Engineering of Sapienza (CNIS), Sapienza University of Rome, Piazzale Aldo Moro 5, 00185 Rome, Italy

HIGHLIGHTS

- A novel, biocompatible smart face mask capable of continuously monitoring respiration and analyzing health data is presented.
- The fabrication process entails the deposition of graphene-based nanocomposite over commercial surgical masks.
- The smart face mask is comfortable, user-friendly, and detects respiration rate without compromising wearability.
- The smart face mask exhibits a fast response time (~42 ms) and long-lasting durability (greater than 1000 cycles).
- The smart face mask communicates to a custom-made mobile App to monitor respiration and send alerts for cough or dyspnea.

GRAPHICAL ABSTRACT

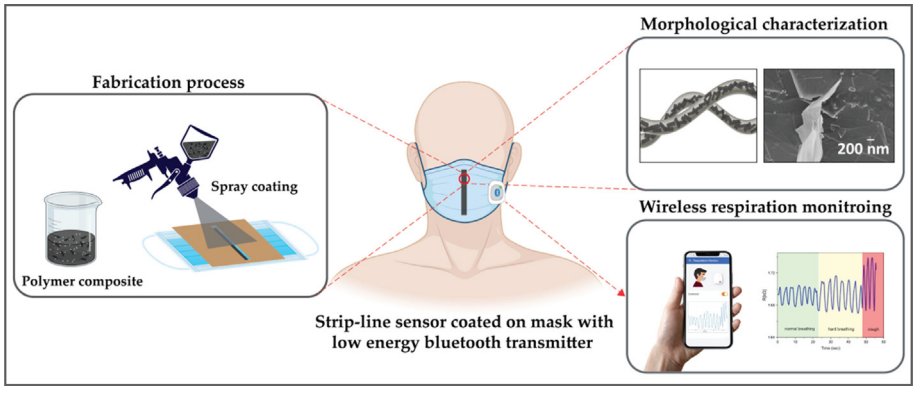

ARTICLE INFO

Article history:
Received 5 October 2022
Revised 20 April 2023
Accepted 26 April 2023
Available online 2 May 2023

Keywords:
Wearable sensing device
Graphene and Advanced materials
Smart face mask
Piezoresistive sensor
Respiration monitoring
Real-time monitoring

ABSTRACT

After the pandemic of SARS-CoV-2, the use of face-masks is considered the most effective way to prevent the spread of virus-containing respiratory fluid. As the virus targets the lungs directly, causing shortness of breath, continuous respiratory monitoring is crucial for evaluating health status. Therefore, the need for a smart face mask (SFM) capable of wirelessly monitoring human respiration in real-time has gained enormous attention. However, some challenges in developing these devices should be solved to make practical use of them possible. One key issue is to design a wearable SFM that is biocompatible and has fast responsivity for non-invasive and real-time tracking of respiration signals. Herein, we present a cost-effective and straightforward solution to produce innovative SFMs by depositing graphene-based coatings over commercial surgical masks. In particular, graphene nanoplatelets (GNPs) are integrated into a polycaprolactone (PCL) polymeric matrix. The resulting SFMs are characterized morphologically, and their electrical, electromechanical, and sensing properties are fully assessed. The proposed SFM exhibits remarkable durability (greater than1000 cycles) and excellent fast response time (~42 ms), providing simultaneously normal and abnormal breath signals with clear differentiation.

* Corresponding author at: Department of Astronautical, Electrical, and Energy Engineering (DIAEE), Sapienza University of Rome, via Eudossiana 18, 00184 Rome, Italy.
E-mail address: hossein.cheraghibidsorkhi@uniroma1.it (H. Cheraghi Bidsorkhi).

https://doi.org/10.1016/j.matdes.2023.111970

Finally, a developed mobile application monitors the mask wearer's breathing pattern wirelessly and provides alerts without compromising user-friendliness and comfort.

1. Introduction

In late 2019, the Covid-19 pandemic quickly spread worldwide and jeopardized global health in more than 200 countries, especially in densely populated areas [1]. Therefore, some global strategies and adequate measures have been made to curb further virus expansions, including hand hygiene, social distancing, wearing a face-mask, and later vaccination. However, at the moment vaccines cannot guarantee complete immunity [2], so face masks are still considered the most effective method for preventing the spread of virus-containing respiratory fluid, which is the primary way of transmission. As the virus attacks the lungs directly, causing symptoms similar to pneumonia and shortness of breath, continuous respiration monitoring is crucial for determining health status as it provides vital information about an individual. Thus, the need for a remote system capable of monitoring the vital sign parameters of the patient has led to the development of smart face-masks (SFMs), allowing healthcare staff to maintain the required distance and constantly control patients' respiration conditions [3,4]. Moreover, in recent years there has been increasing interest in developing these new wearable devices due to their significant advantages compared to traditional respiration monitoring techniques, such as impedance pneumography [5], optical sensors [6], and ballistocardiogram (BCG) [7]. In fact, these conventional methods require expensive, cumbersome structures and external power sources. Furthermore, they lack fast response time, high breathing tracking quality, and user comfort [8]. Hence, the use of SFMs allows us to overcome traditional breath-monitoring systems' limitations and it is believed that it will open the door to many different applications [9].

Briefly, SFMs are designed for two main purposes, both contributing to the control and inhibition of respiratory diseases: (i) evaluating breathing conditions accurately and (ii) improving airborne pathogen filtration, such as the COVID-19 virus [10,11]. Indeed, different single-mode and multi-mode [12] wearable breath sensors for continuous human respiration have been developed. Although multi-modal sensors can detect multi signals and simplify signal processing, their mass production is challenging due to costly materials and fabrication process complexity [12,13]. To date, extensive research has proposed monomodal flexible sensors employing various sensing mechanisms to realize respiration monitoring, including humidity, pressure, and strain.

Many humidity sensors with good stability in the humid environment are designed to track breathing by measuring the relative humidity of exhaled and inhaled air. However, some of them are rigid and realized with metal particles [14–16] or prepared using costly fabrication methods [17,18] or employ interdigitated metallic electrodes [18,19].

Non-self-powered and self-powered pressure sensors have also been utilized for respiration monitoring applications. In non-self-powered prototypes, the need for an external power supply brings some limitations like high cost, complexity, and heavyweight [20,21]. These constraints have been overcome by adopting self-powered pressure sensors based on piezoelectric and electrostatic induction principles [20,22]. However, most existing self-powered sensors do not have easy triggers at low pressure needed in breath monitoring or they are fabricated on a nonporous substrate like Polydimethylsiloxane (PDMS) that is not breathable [3], which hinders the application of SFMs due to heat and discomfort and also cannot obtain a high signal-to-noise ratio in the low-pressure range.

Other piezoresistive pressure sensors consist of 2D-based materials deposited on tissue papers [23], cotton cloth [24] or cellulose fabrics [25]. Conductive polymers such as PANI, are also used [26].

Recently, a new strategy for improving the functionality of SFMs has been proposed by integrating electronic sensors and modules on the inner layer of face masks [11]. This has been made possible by advancements in fabrication techniques that enable the direct printing of functional circuits, whether transient or long-lasting [27]. For instance, a 3D double-arched microstrip antenna [28] has been developed and a radio frequency (RF) transponder has been attached to the inner layer of a surgical mask for cough monitoring [11]. However, the need for transmitting and receiving antennas limits their practical use in daily life.

Besides, improvements have been made in the design of flexible strain sensors that can be used for monitoring [29]. In particular, a strain sensor can be embedded into the structure or attached to the surface. To accomplish strain sensor integration, they are generally fabricated on flexible substrates and then attached to the surface with adhesive or tapes [30,31]. However, these additional materials reduce the user's comfort, wearability, and breathability. An alternative way for sensor integration is to fabricate sensor elements directly on the mask surface [32,33]. Nevertheless, despite intensive research efforts, the direct fabrication of strain sensors on the mask surface has not been fully investigated.

In fact, several authors improved the sensors' performances for continuous and real-time human respiration monitoring; however, these improvements lead to complex manufacturing methods and high production costs [7,19]. Thus, most of the proposed SFMs do not meet some essential standards, such as being fully breathable and biocompatible or realized with a cost-effective production process, suitable for being scaled up to meet industrial requirements.

Herein, a novel, cost-effective, biocompatible, and metal-free SFM is depicted. This SFM is able to detect the breathing rate of the mask-wearing and to recognize abnormal respiration, thus providing alerts in case of cough or shortness of breath. Briefly, piezoresistive graphene-based strip-lines acting as strain sensors are sprayed over the external surface of a commercial surgical mask and the resistance variation due to respiration induced strain is detected and transmitted via Bluetooth to a mobile app that stores and analyses data. The piezoresistive graphene-based strip lines are realized by incorporating graphene nanoplatelets (GNPs) into a polycaprolactone (PCL) polymeric matrix.

GNPs are tiny stacks of graphene layers with a thickness of one to ten nanometres and lateral diameters of up to 10 μm [34]. Due to their cost-effective, ease of fabrication, exceptional mechanical characteristics, and high thermal and electrical conductivities, they have attracted the most interest as nanofillers in polymer composite [35,36]. Furthermore, GNPs show clear hydrophobicity and antimicrobic and antiviral features, that make them particularly suitable to improve airborne pathogen filtration, such as the COVID-19 virus [37]. On the other hand, PCL is known for its biodegradability, biocompatibility, and flexibility [38,39]. The produced SFM clearly detects breathing rates without compromising wearability, breathability, and comfort. Furthermore, owing to GNP hydrophobic properties, the SFM can be washed and reused without properties degradation. Notably, the SFM has the potential to be meritoriously used for the continuous monitoring of human

breath as it presents an excellent fast response time (~42 ms) and remarkable durability, more than 1000 cycles, ensuring its reliability in practical applications.

2. Materials and methods

2.1. Material and fabrication

Commercially available Graphite Intercalation Compound (GIC) is subjected to a thermal shock obtaining worm-like expanded graphite (WEG) [40], as summarized in Fig. 1. After that, WEG is added to a suitable solvent, acetone, and the resulting mixture is sonicated by using an ultrasonic processor for around 40 min in one second on– one second off cycle mode, leading to the WEG exfoliation and obtaining a GNP solution [35]. Then, PCL polymer is added by a ratio of 8 % wt. Successively, the mixture is magnetically stirred for 2 h at a controlled temperature to obtain a homogeneous solution. Finally, the resulting PCL/GNP solution is sprayed on the external surface of a commercial mask using a mold. The obtained graphene-based strip-lines act as strain sensor elements (Fig. 1 (c)).

2.2. Field Emission Scanning electron Microscopy characterization

Surface morphology is analysed using Field Emission Scanning Electron Microscopy (FE-SEM) available at the Sapienza Nanotechnology and Nanoscience laboratory of Sapienza University of Rome (SNN-Lab). The sensors are sputter-coated with a 20 nm chromium layer before acquiring the FE-SEM images. Then, the pure and graphene-coated mask surface morphologies are assessed at different magnifications.

2.3. Contact angle measurement

The hydrophobic behaviour of the pure and graphene-coated mask surfaces is assessed by measuring water contact angles (WCAs). Briefly, ~2 µl of deionized water (DI) are drop-casted on the piezoresistive graphene-based strip-lines acting as sensors and the resulting shape is captured using an optical CA meter available at SNN-Lab. Afterward, the captured images are analysed through ImageJ software, obtaining WCA values.

2.4. Mechanical and electromechanical characterization

The piezoresistive response of the graphene-based strip-lines is evaluated under a quasi-static three-point bend test following the standard ASTM D790-03. The test setup is depicted in Fig. 2**(a)**. This characterization is carried out by applying a mechanical load using the universal testing machine INSTRON 3366. At the same time, the electrical resistance of the graphene-based strip-lines is measured using a Keithley 6221 dc/ac current source and a Keithley 2182a nano voltmeter.

Before conducting this test, the SFMs are cut into three rectangular shapes centred on the graphene-based strip-lines, i.e. sample 1, sample 2, and sample 3. Then, two electrical contacts are realized at both the extremities of the strip-lines as shown in Fig. 2**(a)**.

Initially, a thin silver-paint layer (Electrolube®) is applied to rectangular areas of 4 mm × 2.5 mm. After silver-paint drying, tin-coated copper wires are bonded using a silver-based epoxy adhesive (CircuitWorks®) placed over the contacted areas (0.2 mm in diameter). The films are then cured for 15 min at 30 °C to facilitate the polymerization of the silver-based epoxy adhesive. The so obtained samples are adhered to a 6 mm thick polycarbonate beam, 120 mm long and 24.5 mm wide, with a cyanoacrylate-based adhesive, as graphically represented in Fig. 2 **(b)** [35].

Then, the relative resistance change $\Delta R/R_0$ of each sample is evaluated as the difference between measured resistance R and the initial resistance R_0, divided by R_0. Afterwards, the Gauge Factor (GF) is then obtained from the relative resistance change against the applied mechanical strain [35]:

$$GF = \frac{\Delta R/R_0}{\varepsilon} \tag{1}$$

Successively, in order to evaluate the response time, an instantaneous strain is applied to the produced samples (samples 1,2, and 3), and the response time is measured using a NI-DAQ USB-6001 data acquisition system.

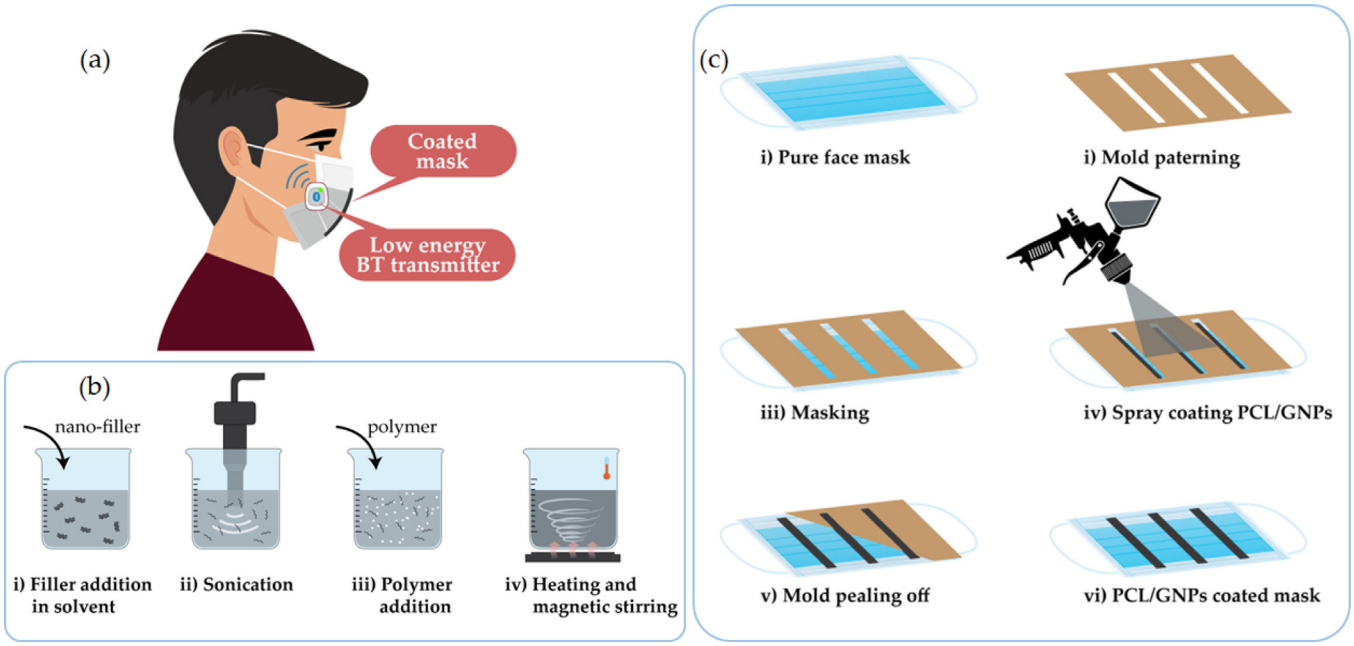

Fig. 1. Proof-of-concept (a); PCL/GNP composite fabrication route (b) and sketch of the steps to spray the PCL-GNP solution over the external surface of a commercial mask (c).

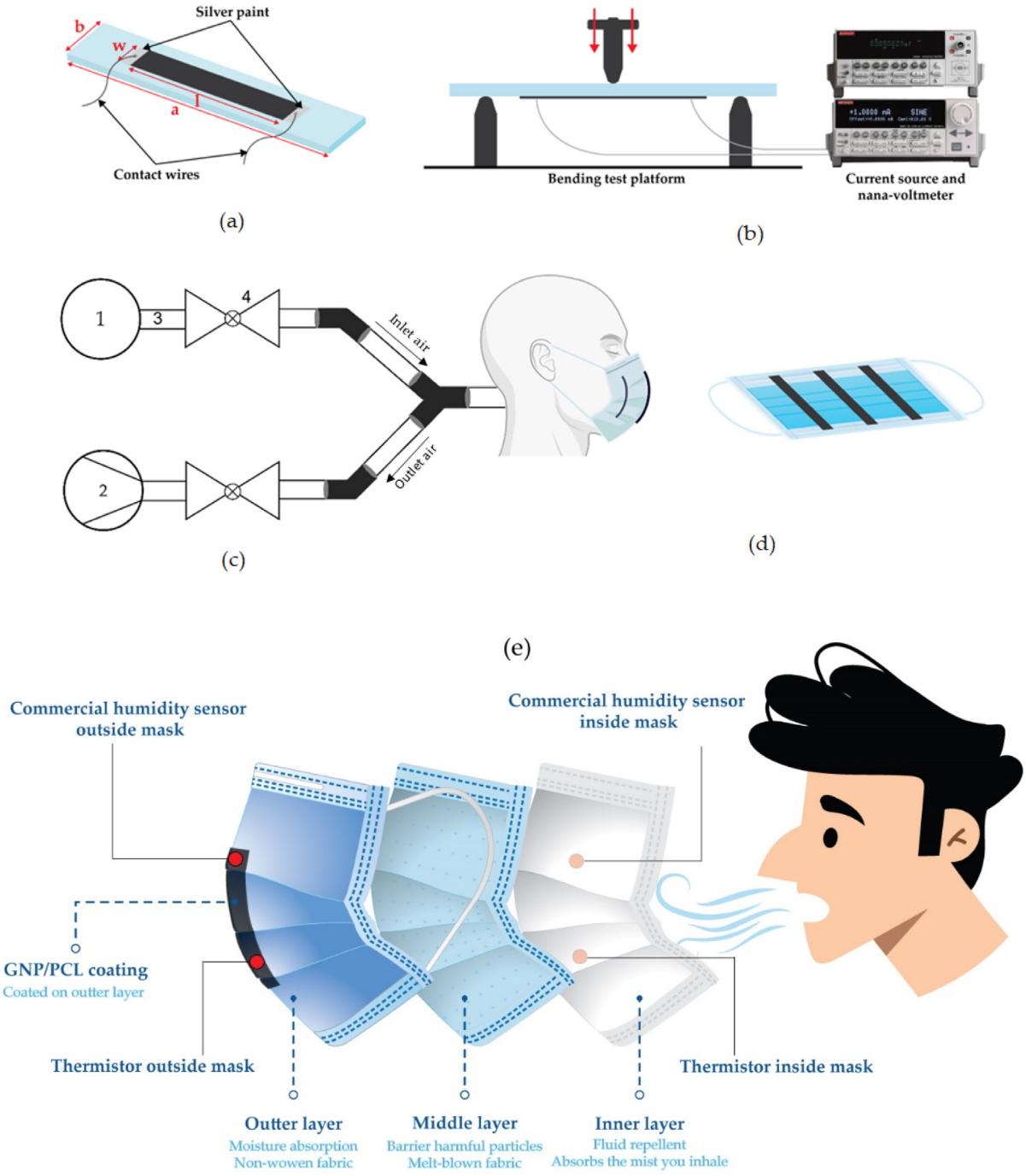

Fig. 2. Graphene-coated strip-line (l = 5 cm, w = 0.5 cm) acting as strain sensor and cast over the external layer of a mask cut into a rectangular shape with dimensions a = 5 cm, b = 0.5 cm and attached on a plexiglass beam (c = 15 cm, and d = 3 cm) (a). Three-point bend test setup at the laboratory (b); Schematic illustration of artificial respiration test setup (*c*); smart face mask with left, center, and right graphene-coated strip-lines (*d*), illustration of the position of the sensor on a three-layer surgical mask (e).

Finally, multicyclic loading–unloading tests are carried out to evaluate the stability and durability of samples for long-term use, recording the piezoresistive response for more than 1000 cycles at a tensile rate of 40 mm/min.

2.5. Artificial respiration test

The artificial respiration test is performed to validate the sensing performance of the SFM by simulating real human breathing. For this purpose, the European Standard EN 14683:2019 + AC [41]is followed and the test set-up sketched in Fig. 2**(c)** is developed. It consists of a vacuum pump and a compressor, connected with a tube connector.

Briefly, the simulation of the exhalation is initiated by turning on the compressor to let the air in and keeping the vacuum pump off. Similarly, the inhalation is simulated by switching on the vacuum pump and switching off the compressor. Then, the air-flow rate, 8 l/min [41], is controlled with valves.

2.6. Wearable smart face mask

The produced SFMs are connected to a real-time data streaming device in order to transmit the detected data to a mobile App. The aim is to constantly monitor wirelessly the breathing condition of the mask wearer and eventually to provide alerts, without compromising the mask's user-friendliness, comfort, and daily life routine of an individual. Hence, a commercial wearable real-time data streaming and logging device MetaMotionS from MBIENTLAB is used for data acquisition of breathing using the graphene-based sensor. This compact device is composed of a Bluetooth Low Energy (BLE) 2.4 GHz transceiver along with 9-axis IMU sensors that operate on a 3 V battery. In addition, the device allows us to interface external sensors with connecting wires.

In this regard, the central graphene-based strip-line is connected to the device in a voltage divider configuration along with a buffer to match the impedance with the Analog-to-Digital Converter (ADC) of the device. An android mobile application is developed to stream and log the data wirelessly from the device through a Bluetooth link. The application receives raw ADC data from the device and performs fundamental digital signal processing to remove noise and smoothen breathing patterns. Eventually, this application can detect abnormal breathing conditions and alarm the user or guardians.

2.7. Exhaled breath temperature and humidity effect in human respiration monitoring

Within the aim of demonstrating that the humidity and temperature of the exhaled breath do not affect the smart mask response, humidity and temperature variations are recorded together with the respiration rate while a volunteer breath. In particular, two commercial humidity sensors and two thermistors are fixed inside and outside the mask, as sketched in Fig. 2**(e)**, and their response is stored and compared with the detected respiration rate.

3. Results and discussion

3.1. Surface morphology

Fig. 3 shows the surface FE-SEM image of the face mask before (Fig. 3(a,b,c)) and after (Fig. 3(d,e,f)) the graphene-based strip-lines are sprayed. From the FE-SEM images of the face mask, the highly porous structure of the polypropylene (PP) fabric is visible. The nonwoven PP fibers, with 20 μm diameter, are located freely and they cross each other. The fibers with an initially smooth surface are uniformly and homogeneously covered with the PCL/GNPs nanostructures. It is obvious that the spray-coated PCL/GNP strip-lines have fully adhered to the fiber surfaces. In addition, as shown in Fig. 3**(d), (e), and (f)**, GNPs fasten flawlessly to the PCL polymer matrix. Moreover, looking at the FE-SEM images it is evident that the spray-coated graphene-based strip-lines do not affect the mask's porous structure, thus they do not compromise the mask's breathability [41]. To assess the SFM's breathability, the air exchange pressure of the medical face mask material can be measured using the setup depicted in **Fig. supplementary (S)1**. The test involves determining the differential pressure necessary to draw air through a defined surface area at a constant rate of airflow [41]. The data acquired through this test indicates that there are minor and insignificant variations in the pressure difference between the uncoated and coated masks, thus demonstrating that the masks remain breathable, even if coated **Fig. supplementary (S)1**. This is an important feature to consider when developing SFMs, as maintaining comfortable and easy breathing for the wearer is crucial for encouraging consistent mask usage and ensuring overall health and safety.

Concerning the working principle of the graphene-based strip-lines acting as strain sensors, it is reasonable to assume that when the strip-lines are subjected to a strain, the distance between overlapped graphene flakes increases, the direct contact area decreases, leading to an increase in the overall electrical resistance during sensor stretching [42–44]. As a consequence, the increase in the piezo-resistive response of the sensor is primarily due to the change in distance between GNPs, as represented in Fig. 3(g,h). In particular, Fig. 3**(g)** depicts the alignment of GNPs in their initial state without deformation. When respiration occurs, the interspace between GNPs in the polymer matrix on the mask fibers increases as shown in Fig. 3**(h)**, and, consequently, the overall resistance increases substantially. Besides, the magnitude of the piezoresistive response is tuned by spray deposition of optimal concentration and distribution of GNPs on the facial mask to produce highly sensitive respiration monitoring sensors.

3.2. Hydrophobic properties

The hydrophobicity of the pure and graphene spray-coated surgical mask sensors is assessed through the CA measurement, as mentioned in Section 2.3. The pure surgical mask CA is reported to have the lowest value of 103 ± 0.3°, as shown in **Fig. supplementary (S)2(a)**, while the CA values for the graphene-coated masks increase to 115 ± 2° for sample 3 **Fig. supplementary (S)2(b)**. In all cases, the water droplets have a semi-circular shape, and despite the lack of a huge increment in CA values, the mask remains hydrophobic while GNP coating improves hydrophobic and antimicrobial properties [45,46] and shown in **Fig. supplementary (S)3**. Therefore, the improved hydrophobic and antimicrobial behaviour of graphene-coated masks can be useful to maintain their performance over more extended periods without affecting their piezoresistive response [40].

3.3. Mechanical and electromechanical characterization

The piezoresistive behaviour is analysed in Fig. 4(a,b,c) in terms of resistance change under structural deformation with the aim of achieving an in-depth electromechanical characterization of the produced graphene-based strip-lines. Each sample is subjected to three consecutive electromechanical tests to determine its repeatability, with a maximum value of up to 0.9 % for strain. The initial resistance values R_0 are acquired before applying strain, i.e., ∼93.65 kΩ for sample1 deposited with lower GNP; ∼31.06 kΩ for sample 2 coated with an intermediate quantity of GNPs; and ∼ 18.99 kΩ for sample 3, obtained with higher amount of GNP. The reported data show an exponential growth of resistance under applied load, with the highest values recorded for sample 1. The piezoresistive effect can be associated with two main dominant mechanisms: (i) disconnection mechanism and (ii) tunneling resistance change due to mechanical deformation [44]. In the first mechanism, overlapped areas among GNPs pave the way for electrons to pass through the percolation network [44]. Under applied strain, the nanomaterials lose their direct connection, leading to decreased overlapped areas and conducting network disruption [47,48]. When the sensor is stretched, sliding graphene flakes in the direction of elongation results in a reduction of overlapped areas between adjacent flakes and, consequently, an increase in contact resistance which contributes to electrical resistance rise [47,49]. Besides, in the tunnelling effect mechanism, electrons can cross through the nonconductive polymer, tunnelling through neighboring nanomaterials [47]. Tunnel resistance increases exponentially with the tunnelling distance, which is proportional to the distance between each GNP and its aggregation, and as a result, the

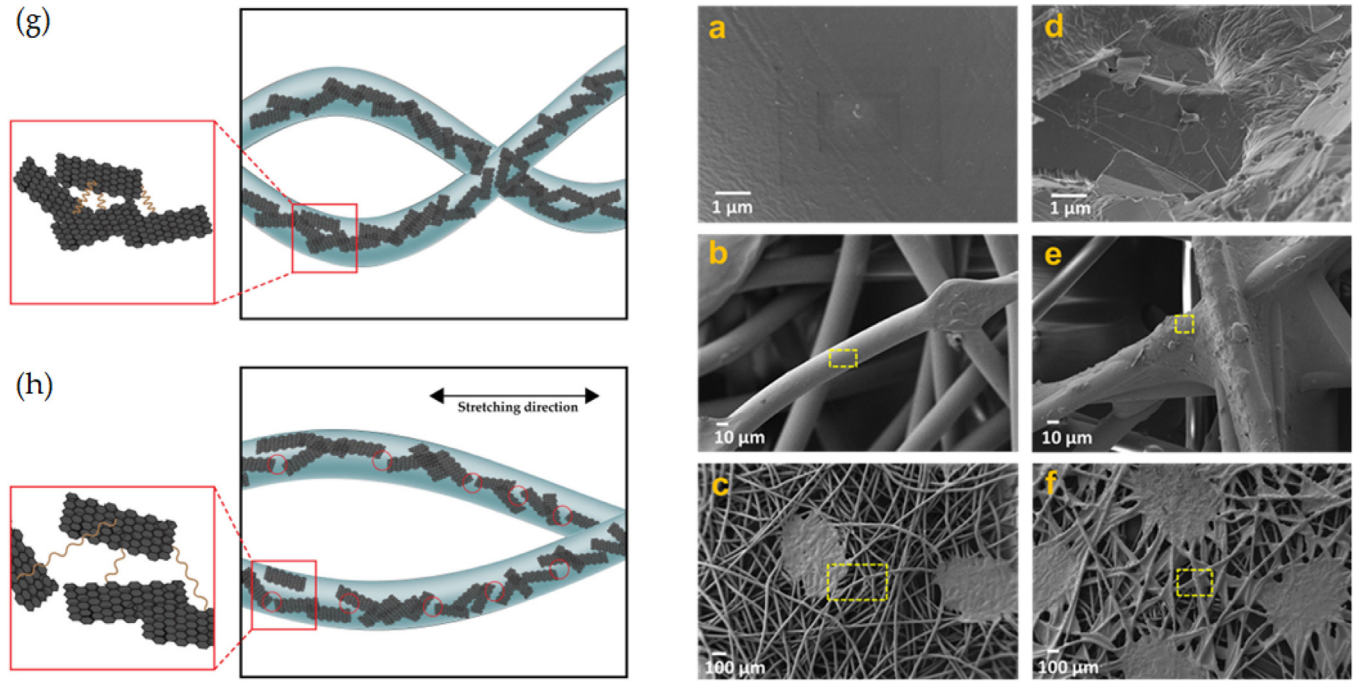

Fig. 3. SEM images, (a,b,c) pure mask, (d,e,f) coated mask, (g) respective schematic illustration of GNPs and polymer bonded to the fibers under no deformation, (h) during inhalation and exhalation.

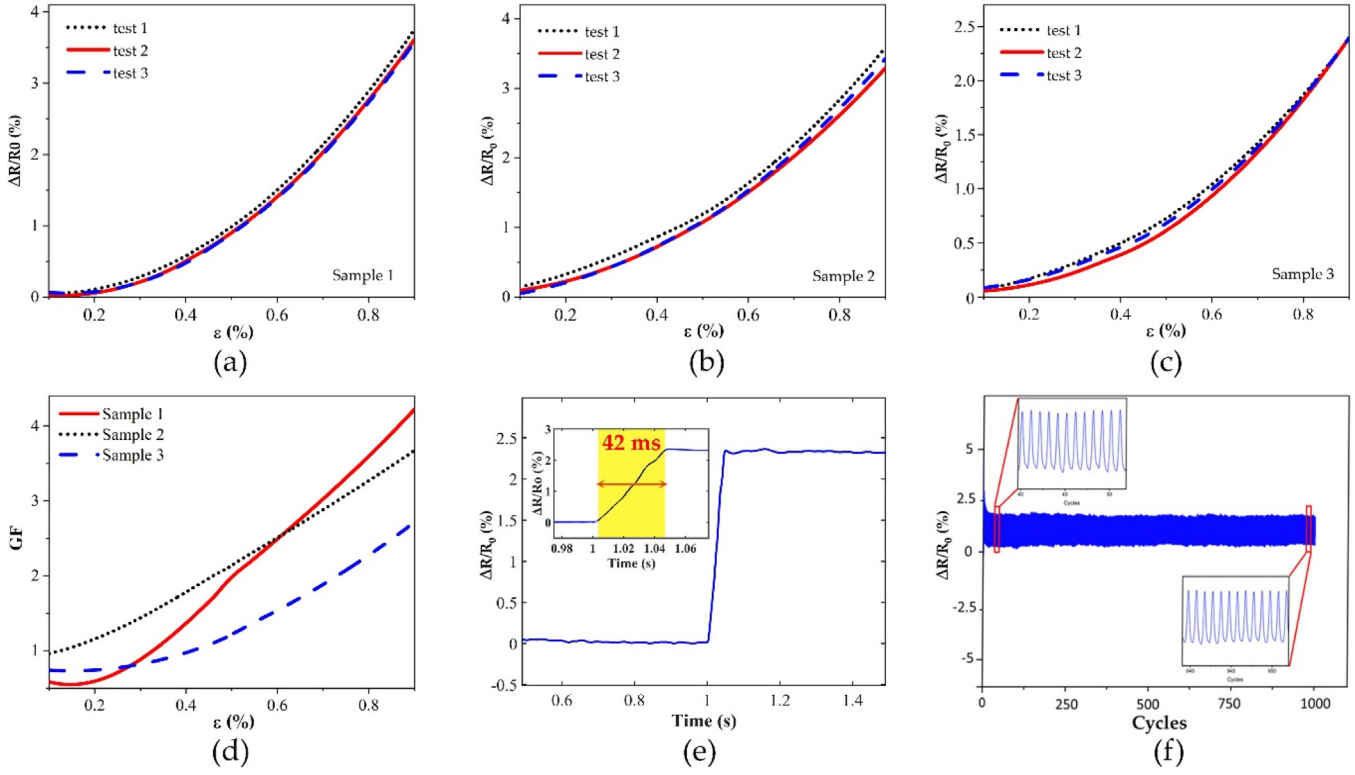

Fig. 4. Relative resistance variation $\Delta R/R_0$ under the applied strain for a graphene-coated face mask (a) sample 1, (b) sample 2, (c) sample 3, and (d) respected gauge factors. Measured average response time (e) and result of reproducibility test when the samples are subjected to long-term use (f).

exponential growth seen in Fig. 4(a,b,c) could be driven by variations in tunnel resistance [35,47,50,51]. The GF, the slope of relative resistance change versus applied strain is reported for all samples in Fig. 6 **(d)**. The maximum value of GF is detected for sample 1 with the value of 4.2, followed by 3.7 and 2.6 for samples 2 and 3, respectively. Notably, the GF's highest value is double that of reported in the literature as a sensor attached to a breathing mask [31]. As expected, the sensitivity is higher in samples having a low GNP content since fewer conduction pathways are present [44,49]. For instance, in sample 1, with a minimum GNP amount

and thus higher electrical resistance, the number of nanofillers to create direct contact pathways is insufficient, so tunnelling conductivity becomes the predominant mechanism [49,51]. Under strain, the tunnelling mechanism is more affected than the direct contact mechanism, which can be the main reason for the exponential tendency of resistance change [52,53]. A lower GNP content network leads to a more effective disconnection between junctions and, consequently, higher GF [47]. However, in higher-content GNP sensors, direct contact among nanomaterials is the reason for connections, which is less affected by strain, so resistance does not change significantly [53]. Furthermore, the area of conductivity (Ac) is a prominent feature of sensitivity. The initial distance between particles, required for tunneling conductivity, increases with Ac, eventually rising strain sensitivity [44].

To further investigate the sensing properties of the samples, more dynamic tests are carried out in order to evaluate the response time and long-term use reproducibility. Fig. 4 (e) depicts the variations in $\Delta R/R_0$ of graphene-based strip-line upon loading until a strain of 5 mm is reached at a strain rate of 400 mm/min and then uploading to initial conditions. An average response time of about 42 ms is detected, indicating a very fast response. In fact, the measured response time is shorter than the ones measured in several developed polymeric strain sensors recently reported in the literature. For instance, the sensor realized with carbonized nano sponge/silicone composites shows a response of ~100 ms [54], the one produced with thermoplastic polyurethane decorated with electrospunned reduced graphene oxide exhibits a response time of ~200 ms [55] while the one presented in [31], consisting of a graphene based layer and a carbon black/single-walled carbon nanotube synergetic conductive network layer shows a response of ~64 ms.

Finally, Fig. 4 (f) shows the behavior of the samples subjected to a durability test by performing loading–unloading at the rate of 4 mm/min. All the samples show excellent reproducibility and stability, indicating that the produced SFMs are suitable for long-term daily use [56].

3.4. Piezo resistive artificial respiration response of SFM

The artificial respiration response of the SFM is evaluated following the procedure described in section 2.6. The SFM is equipped with three graphene-based strip lines acting as strain sensors and located in three different locations to determine the most optimal position for tracking respiration signals: laterals (i.e., left sensor (LS) and right sensor (RS), and central sensor (CS). It is observed that $\Delta R/R_0$ increased during exhale and decreased during inhale, regardless of the sensor's location on the facial mask, as illustrated in Fig. 5 (a,b,-c). As aforementioned in electromechanical tests, an increase in inter-distance between conductive graphene flakes under the deformation causes an increased tunnel resistance; as a result, the electrical resistance increases during exhalation and vice versa for inhalation. Moreover, these respiration waveforms correspond to typical patterns observed in the sensor measurements [57,58].

In particular, sensors LS, RS, and CS are characterized by initial R_0 values, around ~ 61 kΩ, 14.7 kΩ, and 11.5 kΩ, respectively. As previously demonstrated, high sensitivity is achieved by using sensors with low concentrations of GNPs, or in other words, sensors with high initial electrical resistance [35,40]. Due to the fact that the LS and RS are located far from the mouth, detecting mask movement is quite difficult; therefore, increased sensitivity may be required in these positions. As a result, two distinct coatings are chosen: one with a low GNP concentration on LS (i.e., a high GF); and another with a high GNP concentration on RS (i.e., a low GF) comparable to that of CS.

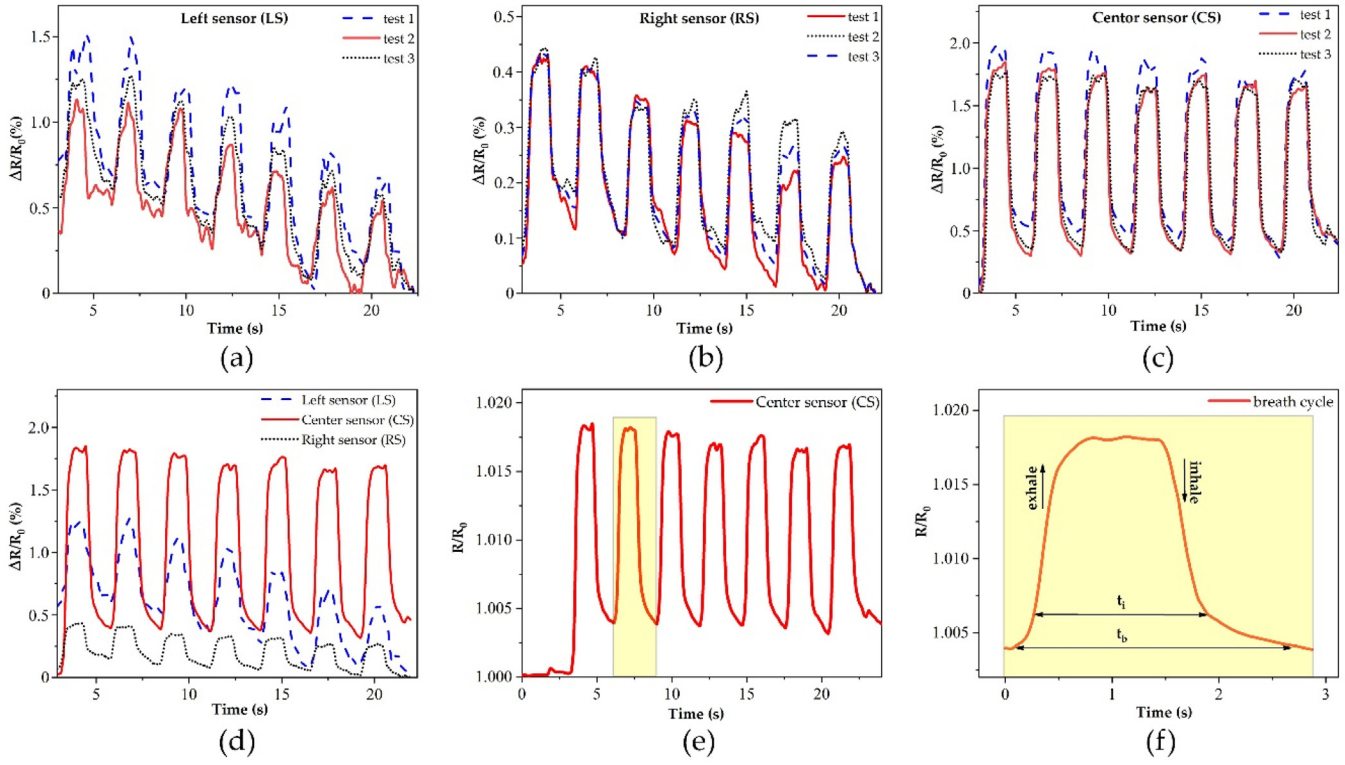

Fig. 5. Relative resistance change ΔR/R0 versus time of artificial respiration test on the graphene-coated surgical mask with three different locations waveforms of (a) Left sensor (LS), (b) Right sensor (RS), (c) Centre sensor (CS), (d) relative average, (e) highlight of the center sensor with second breath cycle, (e) respiration waveform of the single breath cycle highlighted in (f) is magnified.

Although it is estimated that LS is more sensitive due to the low GNP content, the permanent displacement of graphene flakes within the polymer matrix during the initial cycles results in a change in the initial resistance that is not maintained during subsequent breathing cycles, as reported in Fig. 5**(a)**. The RS exhibits a non-uniform and non-repeatable response, despite having a similar GNP deposition layer to the CS, as illustrated in Fig. 5**(b)**. Whereas the central one, which contains also a high concentration of GNP, demonstrates excellent repeatability and sensitivity during measurements, as depicted in Fig. 5**(c)**. The $\Delta R/R_0$ value of CS≈1.7 % is shown in comparison to the LS≈1.25 % and RS≈0.75 % for the initial breathing cycles, as presented in Fig. 5**(d)**. Although the LS and RS have a lower response, they are able to detect mask movement, making this sensor suitable for respiration detection. These plots clearly demonstrate how changes in position and morphological deformation during each measurement affect the response of the LS and RS. Therefore, the drift in the position of the mask during the respiration test is responsible for R_0 variation between successive breathing cycles, and both lateral sensors exhibit a similar descending trend.

As a confirmation, none of these effects are observed in the CS compared to the lateral ones. Indeed, the CS position does not change laterally and is only influenced by breathing. Thus, the CS response is nearly identical and repeatable over time. Hence, the CS is chosen as the optimal location for respiration monitoring. Furthermore, the interval time (t_i), defined as the time between exhalation and inhalation, and the breathing time (t_b), i.e., the time required to complete one breath cycle, are calculated for CS, as highlighted in Fig. 5**(e)** and in the magnified image reported in Fig. 5**(f)**. It yields $t_i \sim 1.62$ s and $t_b \sim 2.86$ s and both valued are within the normal range of healthy young adults [57,58].

The SFMs have also been tested in real-world conditions. In particular, a volunteer person was asked to wear the mask with a central graphene-coated strip-line to continuously monitor respiration signals, as illustrated in Fig. 6**(a)**. The wearable device is attached to the mask as shown in Fig. 6 **(a)**. The application stores the collected data in a text file which can be used later for self-analysis of breathing patterns or transferred to a healthcare specialist for evaluation. As shown in Fig. 6**(b)**, the sensor responds instantly to normal breathing highlighted with a green zone, hard breathing with a red zone, and cough with a yellow zone within the duration of 20 s. The plot depicts that there is a clear differentiation between normal, hard breathing, and cough. It is confirmed that there is an immediate response and magnitude of the $R(\Omega)$ in relation to the intensity of breathing by the volunteer, suggesting that our sensor is suitable to monitor respiration, diagnosing respiratory syndromes such as COVID-19, and providing alerts for patients with abnormalities from their breathing.

To further confirm the practical application of the smart mask, the effect of temperature and humidity is evaluated. It is verified that there is a negligible change in resistance due to humidity change outside of the mask as the inner layer contains and absorbs the exhaled humidity [59]. It is observed that the relative humidity

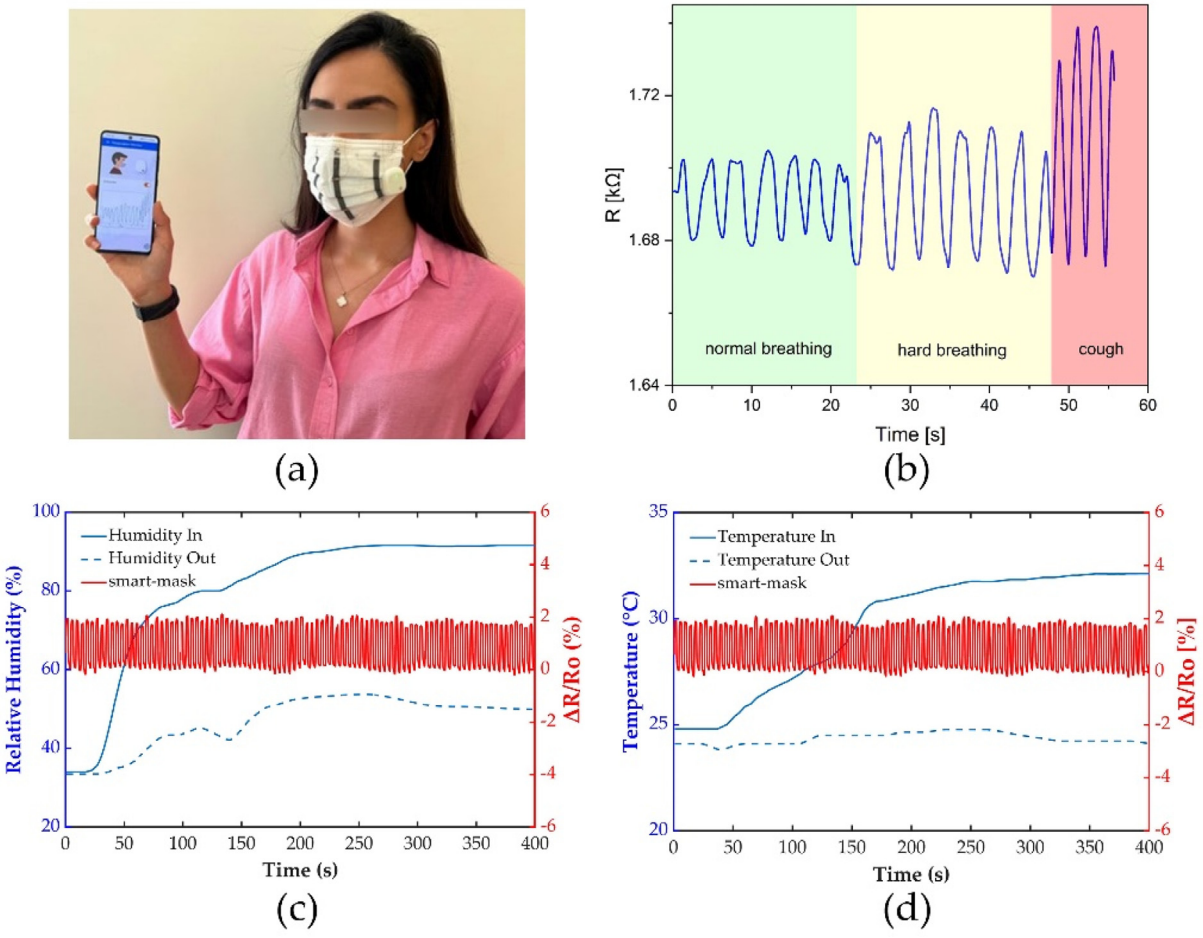

Fig. 6. Illustration of real-time respiration test with smart face mask under wearable application test (a), resistance changes (R)versus time, signals acquired from the volunteer (b), relative resistance change versus temperature change due to breathing inside and outside of the mask (c), relative resistance change versus humidity change due to breathing inside and outside of the mask (d).

rises to 91.6 % inside the mask while breathing. Nonetheless, the humidity just outside the mask rises to 53.6 % in the same period. Reason that the strip-line sensor is coated on the outer layer of the mask, it only corresponds to the ambient humidity changes. Regarding the temperature effect, it is observed that during breathing the temperature outside the mask rises only 3 °C and there is no indication that the sensor's resistance changes as a result of an ambient temperature rise. Regardless, the thermistor detects a change of 7.32 °C inside the mask caused by CO2 emissions, but this has no impact on the performance of the sensor. The experimental data show that the sensor's response remained consistent during both tests (Fig. 6(c,d)).

3.5. Comparison between respiration monitoring sensors and SFMs

Table 1 reports a more comprehensive comparison between some of the most recent respiration monitoring sensors and SFMs recently presented in the literature. Particular emphasis has been given to the sensing principle, response time, fabrication method and flexibility. It is worth to notice that the proposed SFM is the only one realized through direct deposition of the graphene-based strip-line acting as strain sensor over the external surface of a commercial surgical mask, without compromising flexibility and wearability. Furthermore, the proposed SFM is produced through a cost-effective production process and it is characterized by a faster response time with respect to the response times of SFMs and respiration wearable sensors recently reported in the literature. For instance, the graphite carbon nitride/zinc oxide humidity sensor for respiratory monitoring presented in [14] shows a response time of 22 s, even though expensive gold interdigital electrodes are used. In [15] a sensing electronic fabric is developed, however its applicability for respiration monitoring requires its insertion between the inner layers of a surgical mask, which makes it difficult to use with commercially available surgical masks. Additionslly, the proposed prototype requires the incorporation of electronic components, posing potential hazards to the environmental pollution. On the other hand, the textile-based electronic techniques for real-time detection of respiration rate presented in [16] employ critical raw materials such as copper yarns. Then, relatively complex measurement equipment, such as an inductance–capacitance–resistance meter or a vector network analyser, are needed.

A porous graphene based humidity sensors is proposed in [17], however it shows a response time of 31 s which allows the detection of an exhale time of 1.8 s, too high to precisely detect hard coughing or abnormal breathing. Moreover, also in this case, complex production techniques, namely chemical vapour deposition and acid etching, are needed. In [18] a polymeric humidity sensor is developed by depositing electrospun nano-fibers directly onto interdigitated Ag-Pd electrodes, and a minimum response time of 5 s is claimed. The graphdiyne-based flexible respiration sensor presented in [19] employs interdigitated electrodes made of gold. In [20] a SFM designed by integrating an ultrathin self-powered pressure sensor and a compact wireless readout circuit into a normal face mask is proposed. The main drawbacks are: the sensor is not air

Table 1
Comparison between respiration monitoring sensors and smart face masks.

No.	Sensor type	Sensing principle	Sensing material	Response time	Fabrication method	Direct deposition	Flexibility	Note
[14]	Humidity	Capacitive	graphite carbon nitride/zinc oxide	22 s	CVD deposition	No	Semi-Flexible	Expensive production process
[15]	Humidity	Resistive	MXene/MWCNT fabric	28 s	Drop-coating	No	Flexible	Materials are expensive
[16]	Humidity	Capacitive	Yarn combined with copper wire electrodes	3.5 s	Conductive coating on yarn	No	Flexible	Metal-based material
[17]	Humidity	Resistive	graphene/nickel foam	31 s	CVD deposition	No	Semi-Flexible	Expensive production process
[18]	Humidity	Resistive	SPEEK/PVB composite nanofiber	1 s	Electrospinning method, gold electrodes are used as electrodes	No	Rigid	Metal-based material used - expensive production process
[19]	Humidity	Resistive	porous graphdiyne (GDY)	289 ms	Ink-printing method	No	Flexible	——
[20]	Pressure	Piezoelectric	Au/parylene/Teflon AF films	Not reported	CVD method, gold electrodes are used	No	Flexible	Metal-based material- expensive production
[23]	Pressure	Resistive	MXene/tissue paper	150 ms	Screen printing	No	Flexible	
[26]	Pressure	Resistive	PANI-nanospines deposited on a multilayered hierarchicalfibrous structure	Not reported	electron beam (E-beam) evaporation	No	Flexible	Metal-based material
[25]	Pressure	Resistive	carbonized cellulose fabric (CCF)	81 ms	sensor textile manufactured using a Raschel 3D knitting machine	No	Flexible	
[24]	Pressure	Resistive	Ti3C2Tx/NiSe2 hybrid-based pressure sensor on the cotton cloth	220 ms	Oxygen plasma + dip coating in MXene	No	Flexible	Metal-based material
[30]	Strain	Resistive	Aligned nanofibers of ionic liquid (IL)/ thermoplastic polyurethane (TPU) ionogels	119 *m*	Electrospinning method	No	Flexible	
[31]	Strain	Resistive	fiber-based strain sensor covered with GNP layer and a CB/SWCNT synergetic. conductive network layer	65 ms	chemical bonding-based layered dip-coating	No	Flexible	
This work	Strain	Resistive	Graphene/PCL	~42 ms	simple and direct spry coating method	Yes	Flexible	Cost-effective production process

permeable, affecting the permeability of the entire face mask; and the fabrication process is relativity more complicated than that of traditional triboelectric sensors.

A novel flexible paper-based pressure sensing platform that features the MXene-coated tissue paper sandwiched between a polyimide encapsulation layer and a printing paper with interdigital electrodes is presented in [23]. A response time of 150 ms is reached, however incineration is needed for recycling of the silver interdigital electrodes, hence extensive use of this technology may increase the air pollution. Other piezoresistive pressure sensors consist of 2D-based materials deposited on cotton cloth [24] or cellulose fabrics [25]. Conductive polymers such as PANI, are also used [26]. Then, conductive sensor based on fibrous networks [30] or on a synergetic combination of graphene-based nanofillers are attached to the skin or to the external surface of the filters of an air filtration mask [31].

Hence, the proposed SFM is innovative with respect to the state of art since: (i) it clearly and fast detects breathing rate and anomalous breathing conditions without compromising wearability, breathability and comfort; (ii) it exhibits a fast response time (∼42 ms) and long-lasting durability (greater than1000 cycles); (iii) it is realized through an innovative and fast cost-effective production process; (iv) it does not employ metals or other critical raw materials; (v) its production process is suitable to be scaled up, satisfying industrial requirements.

As a final notice, to the best of Authors' knowledge, this SFM is the only one realized through direct deposition of antimicrobial and hydrophobic graphene-based strip-lines acting as sensors over the surface of a commercial surgical mask.

4. Conclusion

In this work, a novel, cost-effective, biocompatible, user-friendly, and metal-free smart face mask is developed, produced, characterized, and tested.

Unlike most of the recently developed smart face masks, which usually employ sensors placed on the mask's internal surface, the proposed SFM is fabricated by depositing graphene-based strip lines acting as sensing elements over the external surface of a commercial surgical mask without compromising the mask's flexibility and wearability.

Briefly, the graphene-based strip lines are realized by dispersing GNPs within a PCL polymer solution and depositing via spray-coating the obtained mixture. Hence, the resulting polymer composite is metal-free, bio-compatible, and green. Then, the production process is cost-effective and scalable to industrial applications.

The graphene-based strip-lines acting as strain sensors show a relatively high sensitivity value under a small strain range of up to 0.9 %, especially considering that no metals or complicated screen-printing techniques or additives were employed. Moreover, it is proven that the graphene-based strip-lines acting as sensing elements show an excellent response time (around 42 ms) and remarkable durability (more than 1000 cycles), ensuring their reliability in practical applications.

Experimentally, it is proven that the produced smart face mask is suitable for continuously monitoring human breathing, distinguishing clearly normal and abnormal breathing rates.

Finally, a mobile App has been realized in order to constantly monitor wirelessly the breathing path of the mask wearer and eventually provide alerts, without compromising the mask user-friendliness, comfort, and daily routine.

Data availability

Data will be made available on request.

Declaration of Competing Interest

The authors declare that they have no known competing financial interests or personal relationships that could have appeared to influence the work reported in this paper.

Acknowledgements

We acknowledge INAIL - Call for BRIC 19 - project NANOBIOSAN for smart mask antibacterial and breathability test. This work has also been supported by LAZIOINNOVA and SAPIExcellence among the research activities of the projects SensE MAsc and MODERN for what concern the smart mask sensorization and the innovative production process respectively.

Appendix A. Supplementary data

Supplementary data to this article can be found online at https://doi.org/10.1016/j.matdes.2023.111970.

References

[1] I. Chakraborty, P. Maity, COVID-19 outbreak: Migration, effects on society, global environment and prevention, Sci. Total Environ. 728 (2020), https://doi.org/10.1016/j.scitotenv.2020.138882.
[2] L. Alexandra, 'Phelan, COVID-19 immunity passports and vaccination certificates: scientific, equitable, and legal challenges, Lancet 395 (2020) 1595–1598.
[3] L. Pan, C. Wang, H. Jin, J. Li, L. Yang, Y. Zheng, Y. Wen, B.H. Tan, X.J. Loh, X. Chen, Lab-on-Mask for Remote Respiratory Monitoring, ACS Mater Lett. 2 (2020) 1178–1181, https://doi.org/10.1021/acsmaterialslett.0c00299.
[4] F. Alshabouna, PEDOT:PSS-modified cotton conductive thread for mass manufacturing of textilebased electrical wearable sensors by computerized embroidery, Mater. Today (2022).
[5] J.J. Freundlich, J.C. Erickson, Electrical Impedance Pneumography for Simple Nonrestrictive Continuous Monitoring of Respiratory Rate, Rhythm and Tidal Volume for Surgical Patients*, n.d.
[6] W. Jae YOO, K. Won JANG, J. Ki SEO, J. Yeon HEO, J. Soo MOON, J. Hoon JUN, J.-Y. Park Ã, B. Lee, Development of Optical Fiber-Based Respiration Sensor for Noninvasive Respiratory Monitoring, n.d.
[7] A. Vehkaoja, A. Kontunen, J. Lekkala, Effects of sensor type and sensor location on signal quality in bed mounted ballistocardiographic heart rate and respiration monitoring, in: Proceedings of the Annual international Conference of the IEEE Engineering in Medicine and Biology Society, EMBS, Institute of Electrical and Electronics Engineers Inc., 2015, pp. 4383–4386, https://doi.org/10.1109/EMBC.2015.7319366.
[8] T. Dinh, T. Nguyen, H.-P. Phan, N.-T. Nguyen, D.V. Dao, J. Bell, Stretchable respiration sensors: Advanced designs and multifunctional platforms for wearable physiological monitoring, Biosens Bioelectron. 166 (2020), https://doi.org/10.1016/j.bios.2020.112460.
[9] N. Panunzio, G.M. Bianco, C. Occhiuzzi, G. Marrocco, RFID sensors for the monitoring of body temperature and respiratory function: A pandemic prospect, 2021 6th International Conference on Smart and Sustainable Technologies, SpliTech 2021, Institute of Electrical and Electronics Engineers Inc., 2021.
[10] R.R. Kalavakonda, N.V.R. Masna, A. Bhuniaroy, S. Mandal, S. Bhunia, A Smart Mask for Active Defense against Coronaviruses and Other Airborne Pathogens, IEEE Consum. Electron. Mag. 10 (2021) 72–79, https://doi.org/10.1109/MCE.2020.3033270.
[11] Z. Ye, Y. Ling, M. Yang, Y. Xu, L. Zhu, Z. Yan, P.Y. Chen, A. Breathable, Reusable, and Zero-Power Smart Face Mask for Wireless Cough and Mask-Wearing Monitoring, ACS Nano 16 (2022) 5874–5884, https://doi.org/10.1021/acsnano.1c11041.
[12] R. Yang, W. Zhang, N. Tiwari, H. Yan, T. Li, H. Cheng, Multimodal Sensors with Decoupled Sensing Mechanisms, Adv. Sci. 9 (26) (2022), https://doi.org/10.1002/advs.202202470.
[13] Z. Pang, Y. Zhao, N. Luo, D. Chen, M. Chen, Flexible pressure and temperature dual-mode sensor based on buckling carbon nanofibers for respiration pattern recognition, Sci Rep. 12 (2022), https://doi.org/10.1038/s41598-022-21572-y.
[14] S. Yu, C. Chen, H. Zhang, J. Zhang, J. Liu, Design of high sensitivity graphite carbon nitride/zinc oxide humidity sensor for breath detection, Sens Actuators B Chem. 332 (2021), https://doi.org/10.1016/j.snb.2021.129536.
[15] H. Xing, X. Li, Y. Lu, Y. Wu, Y. He, Q. Chen, Q. Liu, R.P.S. Han, MXene/MWCNT electronic fabric with enhanced mechanical robustness on humidity sensing for real-time respiration monitoring, Sens Actuators B Chem. 361 (2022), https://doi.org/10.1016/j.snb.2022.131704.
[16] L. Ma, R. Wu, A. Patil, S. Zhu, Z. Meng, H. Meng, C. Hou, Y. Zhang, Q. Liu, R. Yu, J. Wang, N. Lin, X.Y. Liu, Full-Textile Wireless Flexible Humidity Sensor for

Human Physiological Monitoring, Adv Funct Mater. 29 (43) (2019), https://doi.org/10.1002/adfm.201904549.
[17] Y. Pang, J. Jian, T. Tu, Z. Yang, J. Ling, Y. Li, X. Wang, Y. Qiao, H. Tian, Y. Yang, T.L. Ren, Wearable humidity sensor based on porous graphene network for respiration monitoring, Biosens Bioelectron. 116 (2018) 123–129, https://doi.org/10.1016/j.bios.2018.05.038.
[18] X. Li, Z. Zhuang, D. Qi, C. Zhao, High sensitive and fast response humidity sensor based on polymer composite nanofibers for breath monitoring and non-contact sensing, Sens Actuators B Chem. 330 (2021), https://doi.org/10.1016/j.snb.2020.129239.
[19] Y. Li, M. Zhang, X. Hu, L. Yu, X. Fan, C. Huang, Y. Li, Graphdiyne-based flexible respiration sensors for monitoring human health, Nano Today 39 (2021), https://doi.org/10.1016/j.nantod.2021.101214.
[20] J. Zhong, Z. Li, M. Takakuwa, D. Inoue, D. Hashizume, Z. Jiang, Y. Shi, L. Ou, M.O. G. Nayeem, S. Umezu, K. Fukuda, T. Someya, Smart Face Mask Based on an Ultrathin Pressure Sensor for Wireless Monitoring of Breath Conditions, Adv. Mater. 34 (6) (2022), https://doi.org/10.1002/adma.202107758.
[21] Y. Ma, N. Liu, L. Li, X. Hu, Z. Zou, J. Wang, S. Luo, Y. Gao, A highly flexible and sensitive piezoresistive sensor based on MXene with greatly changed interlayer distances, Nat Commun. 8 (2017), https://doi.org/10.1038/s41467-017-01136-9.
[22] X. Peng, K. Dong, C. Ye, Y. Jiang, S. Zhai, R. Cheng, D. Liu, X. Gao, J. Wang, Z. Lin Wang, A breathable, biodegradable, antibacterial, and self-powered electronic skin based on all-nanofiber triboelectric nanogenerators, 2020. https://www.science.org.
[23] L. Yang, H. Wang, W. Yuan, Y. Li, P. Gao, N. Tiwari, X. Chen, Z. Wang, G. Niu, H. Cheng, Wearable Pressure Sensors Based on MXene/Tissue Papers for Wireless Human Health Monitoring, ACS Appl Mater Interfaces. 13 (2021) 60531–60543, https://doi.org/10.1021/acsami.1c22001.
[24] V. Adepu, K. Kamath, V. Mattela, P. Sahatiya, Development of Ti3C2Tx/NiSe2 Nanohybrid-Based Large-Area Pressure Sensors as a Smart Bed for Unobtrusive Sleep Monitoring, Adv Mater Interfaces. 8 (18) (2021), https://doi.org/10.1002/admi.202100706.
[25] H. Choi, J. Sun, B. Ren, S. Cha, J. Lee, B.-M. Lee, J.-J. Park, J.-H. Choi, J.-J. Park, 3D textile structure-induced local strain for a highly amplified piezoresistive performance of carbonized cellulose fabric based pressure sensor for human healthcare monitoring, Chem. Eng. J. 450 (2022), https://doi.org/10.1016/j.cej.2022.138193.
[26] S. Sharma, A. Chhetry, P. Maharjan, S. Zhang, K. Shrestha, M.d. Sharifuzzaman, T. Bhatta, Y. Shin, D. Kim, S. Lee, J.Y. Park, Polyaniline-nanospines engineered nanofibrous membrane based piezoresistive sensor for high-performance electronic skins, Nano Energy 95 (2022), https://doi.org/10.1016/j.nanoen.2022.106970.
[27] N. Yi, Y. Gao, A. Lo Verso, J. Zhu, D. Erdely, C. Xue, R. Lavelle, H. Cheng, Fabricating functional circuits on 3D freeform surfaces via intense pulsed light-induced zinc mass transfer, Mater. Today 50 (2021) 24–34, https://doi.org/10.1016/j.mattod.2021.07.002.
[28] S. Zhang, J. Zhu, Y. Zhang, Z. Chen, C. Song, J. Li, N. Yi, D. Qiu, K. Guo, C. Zhang, T. Pan, Y. Lin, H. Zhou, H. Long, H. Yang, H. Cheng, Standalone stretchable RF systems based on asymmetric 3D microstrip antennas with on-body wireless communication and energy harvesting, Nano Energy 96 (2022), https://doi.org/10.1016/j.nanoen.2022.107069.
[29] L. Yang, C. Liu, W. Yuan, C. Meng, A. Dutta, X. Chen, L. Guo, G. Niu, H. Cheng, Fully stretchable, porous MXene-graphene foam nanocomposites for energy harvesting and self-powered sensing, Nano Energy 103 (2022), https://doi.org/10.1016/j.nanoen.2022.107807 107807.
[30] J. Chen, F. Wang, G. Zhu, C. Wang, X. Cui, M. Xi, X. Chang, Y. Zhu, Breathable Strain/Temperature Sensor Based on Fibrous Networks of Ionogels Capable of Monitoring Human Motion, Respiration, and Proximity, ACS Appl Mater Interfaces. 13 (2021) 51567–51577, https://doi.org/10.1021/acsami.1c16733.
[31] Y. Huang, Y. Zhao, Y. Wang, X. Guo, Y. Zhang, P. Liu, C. Liu, Y. Zhang, Highly stretchable strain sensor based on polyurethane substrate using hydrogen bond-assisted laminated structure for monitoring of tiny human motions, Smart Mater Struct. 27 (3) (2018), https://doi.org/10.1088/1361-665X/aaaba0.
[32] W. Liu, Y. Huang, Y. Peng, M. Walczak, D. Wang, Q. Chen, Z. Liu, L. Li, Stable Wearable Strain Sensors on Textiles by Direct Laser Writing of Graphene, ACS Appl Nano Mater. 3 (2020) 283–293, https://doi.org/10.1021/acsanm.9b01937.
[33] M. Borghetti, M. Serpelloni, E. Sardini, Printed strain gauge on 3D and low-melting point plastic surface by aerosol jet printing and photonic curing, Sensors (Switzerland). 19 (19) (2019), https://doi.org/10.3390/s19194220.
[34] A.G. D'Aloia, H.C. Bidsorkh, G. De Bellis, M.S. Sarto, Graphene based wideband electromagnetic absorbing textiles at microwave bands, IEEE Trans Electromagn Compat. 64 (2022) 710–719, https://doi.org/10.1109/TEMC.2021.3133665.
[35] A. Tamburrano, F. Sarasini, G. De Bellis, A.G. D'Aloia, M.S. Sarto, The piezoresistive effect in graphene-based polymeric composites, Nanotechnology 24 (46) (2013), https://doi.org/10.1088/0957-4484/24/46/465702.
[36] H. Huang, S. Su, N. Wu, H. Wan, S. Wan, H. Bi, L. Sun, Graphene-based sensors for human health monitoring, Front Chem. 7 (2019), https://doi.org/10.3389/fchem.2019.00399.
[37] Á. Serrano-Aroca, K. Takayama, A. Tuñón-Molina, M. Seyran, S.S. Hassan, P. Pal Choudhury, V.N. Uversky, K. Lundstrom, P. Adadi, G. Palù, A.A.A. Aljabali, G. Chauhan, R. Kandimalla, M.M. Tambuwala, A. Lal, T.M. Abd El-Aziz, S. Sherchan, D. Barh, E.M. Redwan, N.G. Bazan, Y.K. Mishra, B.D. Uhal, A. Brufsky, Carbon-Based Nanomaterials: Promising Antiviral Agents to Combat COVID-19 in the Microbial-Resistant Era, ACS Nano 15 (5) (2021) 8069–8086, https://doi.org/10.1021/acsnano.1c00629.
[38] M.J. Mochane, T.S. Motsoeneng, E.R. Sadiku, T.C. Mokhena, J.S. Sefadi, Morphology and properties of electrospun PCL and its composites for medical applications: A mini review, Applied Sciences (Switzerland). 9 (11) (2019), https://doi.org/10.3390/app9112205.
[39] K. Liu, J. Wang, S. Fang, H. Wang, Y. Bai, Z. Zhao, Q. Zhu, C. Wang, G. Chen, H. Jiang, J. Sun, P. Zhang, Effect of polycaprolactone impregnation on the properties of calcium silicate scaffolds fabricated by 3D printing, Mater Des. 220 (2022), https://doi.org/10.1016/j.matdes.2022.110856.
[40] H. Cheraghi Bidsorkhi, A.G. D'Aloia, A. Tamburrano, G. De Bellis, M.S. Sarto, Waterproof graphene-pvdf wearable strain sensors for movement detection in smart gloves, Sensors 21 (16) (2021), https://doi.org/10.3390/s21165277.
[41] EN14683:2019+AC, EN 14683:2019+AC:2019 Medical face masks - Requirements and test methods, (2019) 26., (n.d.).
[42] M. Hempel, D. Nezich, J. Kong, M. Hofmann, A novel class of strain gauges based on layered percolative films of 2D materials, Nano Lett. 12 (2012) 5714–5718, https://doi.org/10.1021/nl302959a.
[43] L.Q. Tao, D.Y. Wang, H. Tian, Z.Y. Ju, Y. Liu, Y. Pang, Y.Q. Chen, Y. Yang, T.L. Ren, Self-adapted and tunable graphene strain sensors for detecting both subtle and large human motions, Nanoscale 9 (2017) 8266–8273, https://doi.org/10.1039/c7nr01862b.
[44] M. Bragaglia, L. Paleari, F.R. Lamastra, D. Puglia, F. Fabbrocino, F. Nanni, Graphene nanoplatelet, multiwall carbon nanotube, and hybrid multiwall carbon nanotube–graphene nanoplatelet epoxy nanocomposites as strain sensing coatings, J. Reinf. Plast. Compos. 40 (2021) 632–643, https://doi.org/10.1177/0731684421994324.
[45] S. Syama, P.V. Mohanan, Comprehensive Application of Graphene: Emphasis on Biomedical Concerns, Nanomicro Lett. 11 (2019), https://doi.org/10.1007/s40820-019-0237-5.
[46] J. Gong, H. Tang, M. Wang, X. Lin, K. Wang, J. Liu, Novel three-dimensional graphene nanomesh prepared by facile electro-etching for improved electroanalytical performance for small biomolecules, Mater Des. 215 (2022), https://doi.org/10.1016/j.matdes.2022.110506.
[47] M. Amjadi, K.U. Kyung, I. Park, M. Sitti, Stretchable, Skin-Mountable, and Wearable Strain Sensors and Their Potential Applications: A Review, Adv Funct Mater. 26 (2016) 1678–1698, https://doi.org/10.1002/adfm.201504755.
[48] S. Zhao, P. Zheng, Q. Liu, L.i. Niu, H. Cong, A. Wan, Highly stretchable strain sensor with tunable sensitivity via polydopamine template-assisted dual-mode cooperative conductive network for human motion detection, Mater Des. 206 (2021), https://doi.org/10.1016/j.matdes.2021.109780.
[49] M. Amjadi, Y.J. Yoon, I. Park, Ultra-stretchable and skin-mountable strain sensors using carbon nanotubes-Ecoflex nanocomposites, Nanotechnology 26 (37) (2015), https://doi.org/10.1088/0957-4484/26/37/375501.
[50] N. Hu, Y. Karube, C. Yan, Z. Masuda, H. Fukunaga, Tunneling effect in a polymer/carbon nanotube nanocomposite strain sensor, Acta Mater. 56 (2008) 2929–2936, https://doi.org/10.1016/j.actamat.2008.02.030.
[51] R. Moriche, M. Sánchez, A. Jiménez-Suárez, S.G. Prolongo, A. Ureña, Strain monitoring mechanisms of sensors based on the addition of graphene nanoplatelets into an epoxy matrix, Compos Sci Technol. 123 (2016) 65–70, https://doi.org/10.1016/j.compscitech.2015.12.002.
[52] O. Kanoun, C. Müller, A. Benchirouf, A. Sanli, T.N. Dinh, A. Al-Hamry, L. Bu, C. Gerlach, A. Bouhamed, Flexible carbon nanotube films for high performance strain sensors, Sensors (Switzerland). 14 (2014) 10042–10071, https://doi.org/10.3390/s140610042.
[53] C. Lee, L. Jug, E. Meng, High strain biocompatible polydimethylsiloxane-based conductive graphene and multiwalled carbon nanotube nanocomposite strain sensors, Appl Phys Lett. 102 (18) (2013), https://doi.org/10.1063/1.4804580.
[54] X.G. Yu, Y.Q. Li, W. Bin Zhu, P. Huang, T.T. Wang, N. Hu, S.Y. Fu, A wearable strain sensor based on a carbonized nano-sponge/silicone composite for human motion detection, Nanoscale 9 (2017) 6680–6685, https://doi.org/10.1039/c7nr01011g.
[55] Y. Wang, J. Hao, Z. Huang, G. Zheng, K. Dai, C. Liu, C. Shen, Flexible electrically resistive-type strain sensors based on reduced graphene oxide-decorated electrospun polymer fibrous mats for human motion monitoring, Carbon N Y. 126 (2018) 360–371, https://doi.org/10.1016/j.carbon.2017.10.034.
[56] Y. Zheng, Y. Li, Y. Zhou, K. Dai, G. Zheng, B. Zhang, C. Liu, C. Shen, High-Performance Wearable Strain Sensor Based on Graphene/Cotton Fabric with High Durability and Low Detection Limit, ACS Appl Mater Interfaces. 12 (2020) 1474–1485, https://doi.org/10.1021/acsami.9b17173.
[57] K.H. Chon, S. Dash, K. Ju, Estimation of Respiratory Rate From Photoplethysmogram Data Using Time-Frequency Spectral Estimation, IEEE Trans Biomed Eng. 56 (2009) 2054–2063, https://doi.org/10.1109/TBME.2009.2019766.
[58] L. Nilsson, T. Goscinski, A. Johansson, L.G. Lindberg, S. Kalman, Age and gender do not influence the ability to detect respiration by photoplethysmography, J Clin Monit Comput. 20 (2006) 431–436, https://doi.org/10.1007/s10877-006-9050-z.
[59] F. Seidi, C. Deng, Y. Zhong, Y. Liu, Y. Huang, C. Li, H. Xiao, Functionalized Masks: Powerful Materials against COVID-19 and Future Pandemics, Small 17 (42) (2021), https://doi.org/10.1002/smll.202102453.